2

Dampers and Vehicle Modelling

2.1 Introduction

The heart of a semi-active suspension is the controllable damper. Its accurate modelling is crucial for suspension analysis and design. In many practical applications the damper characteristic exhibits a strong non-linearity, which must be taken into account in simulation studies in order to obtain realistic results when investigating system performance.

A damper is identified by its force versus velocity characteristics (damping characteristics or hydraulic characteristics), which can be expressed by the functional relation

$$F_d = f(\dot{x}), \tag{2.1}$$

F_d being the damping force generated and $\dot{x}$ the velocity across it. Other damping elements have a more general non-linear characteristics expressed by the functional relation

$$F_d = f(x,\dot{x}). \tag{2.2}$$

Such a characteristic is typical of viscoelastic materials, but it could well represent a controlled semi-active damper, whilst generalised semi-active damping devices can be made to have a characteristic expressed by

$$F_d = f(x,\dot{x},\ddot{x}) \tag{2.3}$$

with acceleration-dependent damping too.

A certain amount of hysteresis is always present in a damper characteristic, depending upon its internal dissipation mechanism. As introduced in Chapter 1 a

damper can be viewed from an energy standpoint as a device that dissipates energy through an internal mechanism (*e.g.*, by throttling a viscous flow through an orifice). In order to fully identify a damper, besides its damping characteristics it is customary to define also its force versus displacement characteristics (damper work characteristics), the area of which gives a measure of the energy dissipated over a complete cycle.

This chapter presents the mathematical techniques necessary to model real dampers with hysteresis in their characteristics, and subsequently reviews the main car and truck ride models, developed for suspension studies. The last part of the chapter deals with road modelling.

Figures 2.1 and 2.2 plot the characteristics of two types of dampers: an ideal linear viscous damper and an ideal Coulomb friction damper. These are idealised characteristics as no hysteresis is present in the force versus velocity characteristics (real dampers always contain a certain amount of hysteresis in their force versus velocity map).

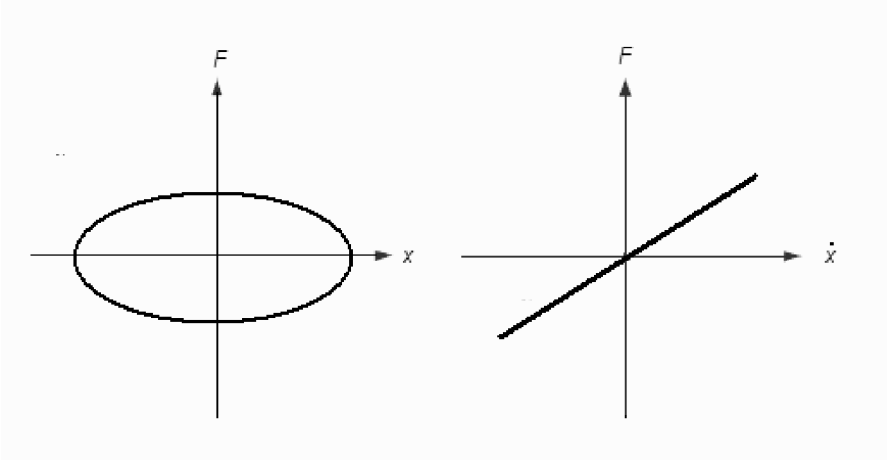

Fig. 2.1. Linear viscous damper characteristics

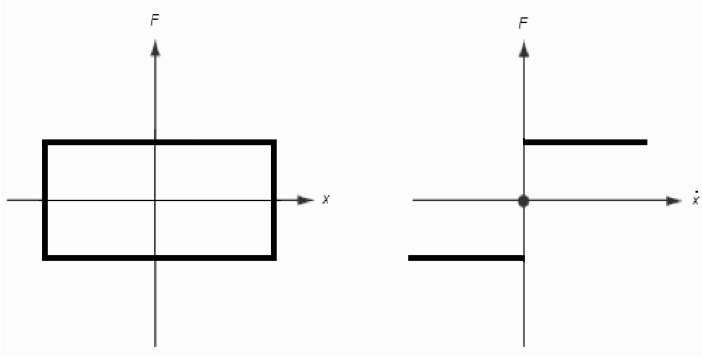

Fig. 2.2. Coulomb friction damper characteristics

2.2 Phenomenology of Hysteresis

Hysteresis occurs in a variety of physical systems; the most noteworthy examples are ferromagnetic materials, constituting the core of motors, generators, transformers and a wide range of other electrical devices. In automotive applications hysteresis is present not only in damper characteristics but also, for instance, in tyre characteristics and in all viscoelastic and viscoplastic materials in general.

From a control systems standpoint, hysteresis must not always be regarded as a non-linearity hampering controller performance or making its design more difficult. Under particular circumstances hysteresis can be beneficially exploited in control systems, namely in on–off control algorithms (Gerdes and Hedrick, 1999) for reducing chatter which may occur when in a control loop the difference between setpoint and feedback (*i.e.*, the error) is close to zero. In such systems the required amount of hysteresis is typically generated within the control software in microprocessor-based programmable architectures or in hardware by employing electronic devices or exploiting the inherent hysteresis present in actuator characteristics (*e.g.*, valves).

Virtually no material or device employed in mechanical and structural systems is perfectly elastic, and restoring forces generated as a result of deformations are not perfectly conservative. Likewise internal dissipation within viscous fluids in dampers result in a hysteretic characteristic.

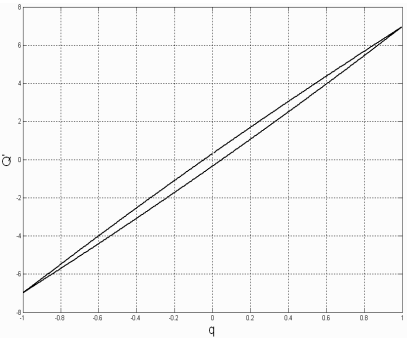

Fig. 2.3. Typical hysteretic loop for a linear material (copyright Publishing House of the Romanian Academy (2002), reproduced from Giuclea M, Sireteanu T, Mita AM, Ghita G, Genetic algorithm for parameter identification of Bouc–Wen model, Rev Roum Sci Techn Mec Appl, Vol 51, N 2, pp 179–188, used by permission)

A wide variety of micromechanisms contribute to energy dissipation in cyclically loaded materials and in viscous fluids. This behaviour macroscopically results in a hysteretic loop when the material or device is subject to a sinusoidal displacement Q'. However, it is not possible — except in very special cases — to quantitatively predict the macroscopic hysteretic behaviour starting from physical models of the microscopic behaviour. Therefore, from an engineering standpoint, an experimental assessment of the hysteresis loop and the corresponding energy losses

is required to characterise a material. Figures 2.3, 2.4 and 2.5 depict typical hysteretic loops for a linear material, a non-linear hardening material and a non-linear softening material, respectively.

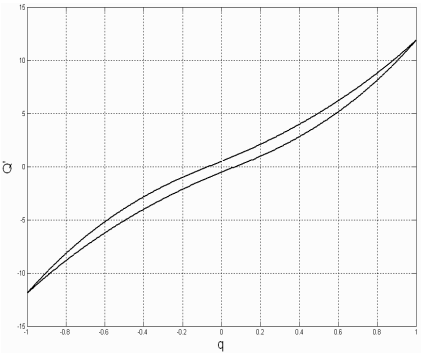

Fig. 2.4. Typical hysteretic loop for a non-linear hardening material (copyright Publishing House of the Romanian Academy (2002), reproduced from Giuclea M, Sireteanu T, Mita AM, Ghita G, Genetic algorithm for parameter identification of Bouc–Wen model, Rev Roum Sci Techn Mec Appl, Vol 51, N 2, pp 179–188, used by permission)

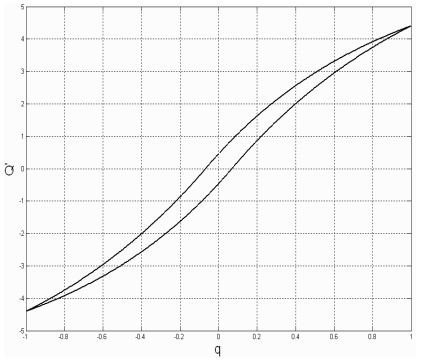

Fig. 2.5. Typical hysteretic loop for a non-linear softening material (copyright Publishing House of the Romanian Academy (2002), reproduced from Giuclea M, Sireteanu T, Mita AM, Ghita G, Genetic algorithm for parameter identification of Bouc–Wen model, Rev Roum Sci Techn Mec Appl, Vol 51, N 2, pp 179–188, used by permission)

The area enclosed by the loop is a measure of the dissipated energy. The area, and hence the energy dissipated per cycle, can be calculated by the following contour integral:

$$E = \oint Q' \, \mathrm{d}q \, . \tag{2.4}$$

Depending upon the material, the hysteresis loop can be either very thin (and generally elliptical in shape), resulting in a very small amount of energy dissipation (Figure 2.6) or larger, hence producing a more significant energy consumption.

Thin loops are likely to occur in elastic materials, such as steel, when they are cyclically loaded within their elastic range. Conversely, materials loaded in their inelastic range exhibit wider hysteresis loops, as portrayed in Figure 2.7. Composite materials too dissipate significant amounts of energy.

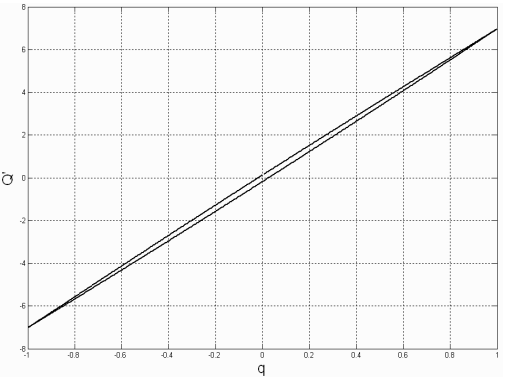

Fig. 2.6. Deformation in the elastic range (copyright Publishing House of the Romanian Academy (2002), reproduced from Giuclea M, Sireteanu T, Mita AM, Ghita G, Genetic algorithm for parameter identification of Bouc–Wen model, Rev Roum Sci Techn Mec Appl, Vol 51, N 2, pp 179–188, used by permission)

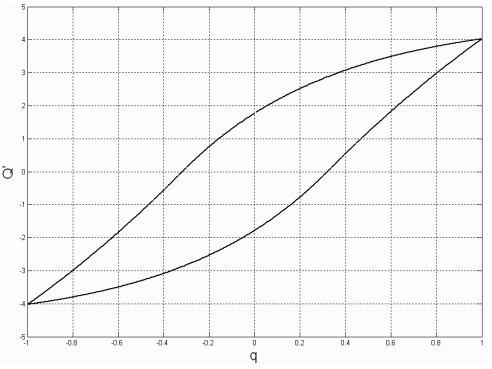

Fig. 2.7. Deformation in the plastic range (copyright Publishing House of the Romanian Academy (2002), reproduced from Giuclea M, Sireteanu T, Mita AM, Ghita G, Genetic algorithm for parameter identification of Bouc–Wen model, Rev Roum Sci Techn Mec Appl, Vol 51, N 2, pp 179–188, used by permission)

A loss function $L(E)$ can therefore be defined for a particular material or damping device under a sinusoidal load. Measuring the area enclosed by the hysteretic loop, and dividing it by the cycle period T, the average energy loss per cycle can be obtained

$$L(E) = \frac{1}{T}\int_0^T Q'\,\dot{q}\,\mathrm{d}t\,. \tag{2.5}$$

2.3 Damper Hysteresis Modelling

The energy dissipation and the impact on control systems performance of hysteretic materials can be significant and in order to properly assess the system response the availability of a control-oriented easy-to-handle analytical model of hysteresis is fundamental.

Hysteresis modelling has been a challenging problem for engineers, physicists and mathematicians. Several models have been proposed over the years to capture different classes of hysteretic phenomena using a variety of approaches. Some models require an in-depth knowledge of specialist areas of mathematics to be fully appreciated. A survey can be found in Mayergoyz (1991), in Visintin (1994) and in Sain *et al.* (1997). Amongst the hysteresis models developed it is worth citing the Chua–Stromsoe model (Chua and Bass, 1972) and the Hysteron model proposed by Krasnoel´skii and Pokrovskii (1989). Another model, known as the Preisach model (Brokate and Visintin, 1989) exists, constructed by superposing the outputs of a set of hysteretic relays. Other models have been proposed, including hysteretic biviscous models (Wereley *et al.*, 1998) and polynomial models (Choi *et al.*, 2001).

A model having an appealing simplicity is the Bouc–Wen model, which has gained large consensus within the engineering community. A wide variety of hysteretic shapes can be represented by using this simple differential model proposed by Bouc (1971) and generalised by Wen (1976). The model is based on a nonlinear ordinary differential equation which contains a memory variable z, representing (in the case of a damping system) the hysteretic restoring force, the position of which is identified by the variable q. The Bouc–Wen equation is defined as follows (Sain *et al.*, 1997): given $T = [t_0, t] \in \Re$, the states $q(t)$, $z(t)$: $T \to \Re$, a vector-valued function $f : (\Re^m, \Re^m, \Re, \Re) \to \Re^m$ and the input $u(t)$: $T \to \Re$, the Bouc–Wen model is defined by:

$$\ddot{q}(t) = f(q, \dot{q}, z, u) \qquad \ddot{q}(t_0) = q_0, \tag{2.6a}$$

$$\dot{z} = -\gamma |\dot{q}| z |z|^{n-1} - \nu \dot{q} |z|^n + A\dot{q} \qquad z(t_0) = z_0, \tag{2.6b}$$

where q is the imposed displacement of the device (or the material deformation). The quantities γ, ν, A, n are loop parameters defining the shape and the amplitude of the hysteresis loop.

Figures 2.8, 2.9 and 2.10 depicts three typical hysteretic loops plotted for different sets of parameters and for an imposed harmonic displacement $q(t)=q_0\sin(2\pi ft)$, where f =1 Hz is the frequency and q_0 is the amplitude of the sinusoidal input.

By consideration of the three Figures 2.8, 2.9 and 2.10 it can be seen that the Bouc–Wen equation can describe both linear and non-linear (softening and hardening) hysteretic behaviour.

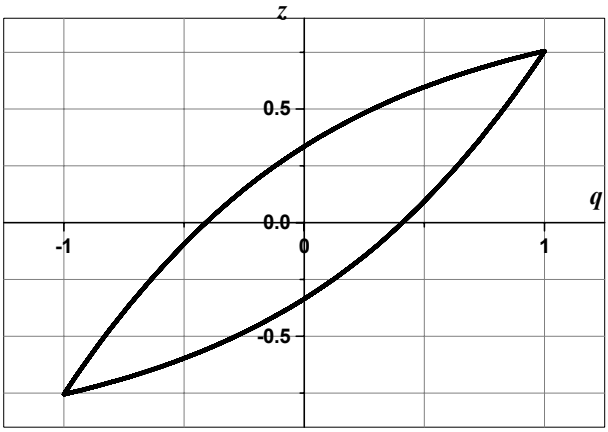

Fig. 2.8. Linear hysteretic behaviour, plotted for $\gamma = 0.9$, $\nu = 0$, $A = 1$, $n = 1$ (copyright Publishing House of the Romanian Academy (2002), reproduced from Giuclea M, Sireteanu T, Mita AM, Ghita G, Genetic algorithm for parameter identification of Bouc–Wen model, Rev Roum Sci Techn Mec Appl, Vol 51, N 2, pp 179–188, used by permission)

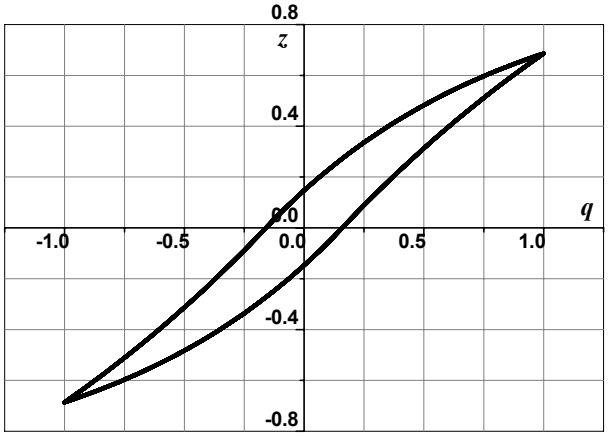

Fig. 2.9. Non-linear softening hysteretic behaviour, plotted for $\gamma = 0.75$, $\nu = 0.25$, $A = 1$, $n = 1$ (copyright Publishing House of the Romanian Academy (2002), reproduced from Giuclea M, Sireteanu T, Mita AM, Ghita G, Genetic algorithm for parameter identification of Bouc–Wen model, Rev Roum Sci Techn Mec Appl, Vol 51, N 2, pp 179–188, used by permission)

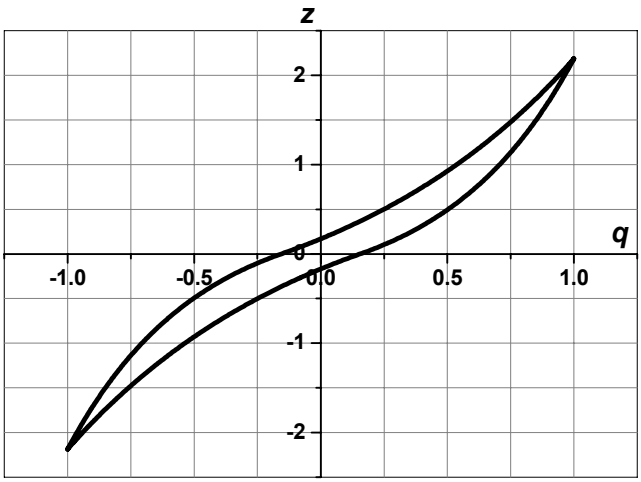

Fig. 2.10. Non-linear hardening hysteretic behaviour (plotted for $\gamma = 0.5$, $\nu = -1.5$, $A = 1$, $n = 1$) (copyright Publishing House of the Romanian Academy (2002), reproduced from Giuclea M, Sireteanu T, Mita AM, Ghita G, Genetic algorithm for parameter identification of Bouc–Wen model, Rev Roum Sci Techn Mec Appl, Vol 51, N 2, pp 179–188, used by permission)

2.3.1 Bouc–Wen Model

This section describes how the Bouc–Wen equation coefficients γ, ν, A and n affect the shape and the amplitude of hysteretic loops. It will be shown how these parameters define the slope rate and the stiffness (linear, hardening or softening) of the characteristics and hence the area (and therefore the energy dissipated over a cycle). The following results are based on a numerical analysis as it is extremely difficult to define analytical correlations due to the non-linearity of the Bouc–Wen equation.

2.3.1.1 Parameter A

As it can be evinced from Figure 2.11, the parameter A defines the scale and the amplitude of the hysteretic curve and the slope of the variation of the stiffness characteristic. An increase in the parameter A results in a wider hysteresis loop, and consequently in a larger energy dissipation.

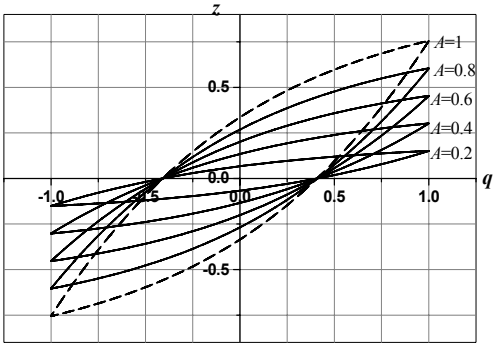

Fig. 2.11. Hysteretic loop dependence on the parameter A (plotted for $\gamma = 0.9$, $\nu = 0.1$, $n = 1$) (copyright Publishing House of the Romanian Academy (2002), reproduced from Giuclea M, Sireteanu T, Mita AM, Ghita G, Genetic algorithm for parameter identification of Bouc–Wen model, Rev Roum Sci Techn Mec Appl, Vol 51, N 2, pp 179–188, used by permission)

2.3.1.2 Parameter γ

The dependence of the hysteretic loops on the parameter γ is portrayed in Figure 2.12 (plotted for $\nu = 0.1$, $n = 1$, $A = 1$) and can be summarised by saying that the area of the loop increases if γ increases from 0 to a value γ_0 (between 2 and 3 in the numerical example of Figure 2.12, but in general dependent on the other coefficients), and for values of γ larger than γ_0 the energy dissipated per cycle slightly decreases.

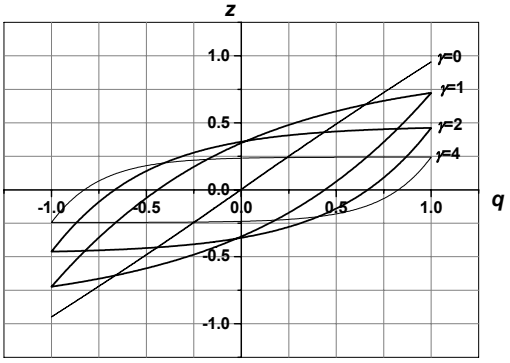

Fig. 2.12. Hysteretic loop dependence on the parameter γ (plotted for $\nu = 0.1$, $n = 1$, $A = 1$) (copyright Publishing House of the Romanian Academy (2002), reproduced from Giuclea M, Sireteanu T, Mita AM, Ghita G, Genetic algorithm for parameter identification of Bouc–Wen model, Rev Roum Sci Techn Mec Appl, Vol 51, N 2, pp 179–188 used by permission)

2.3.1.3 Parameter ν

It can be noticed (Figure 2.13) that the parameter ν controls the shape of the hysteretic curve: $\nu = 0$ corresponds to a linear hysteretic behaviour, $\nu < 0$ produces a hardening hysteretic behaviour, and $\nu > 0$ results in a softening hysteretic behaviour.

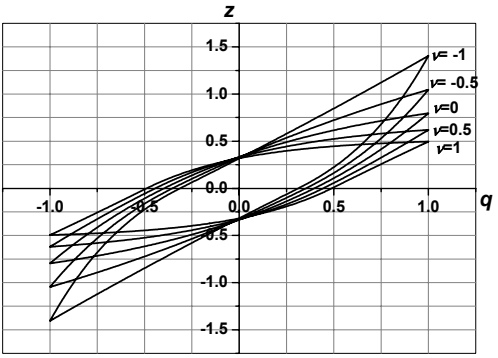

Fig. 2.13. Hysteretic loop dependence on the parameter ν (plotted for $\gamma = 0.9$, $n = 1$, $A = 1$) (copyright Publishing House of the Romanian Academy (2002), reproduced from Giuclea M, Sireteanu T, Mita AM, Ghita G, Genetic algorithm for parameter identification of Bouc–Wen model, Rev Roum Sci Techn Mec Appl, Vol 51, N 2, pp 179–188, used by permission)

2.3.1.4 Parameter n

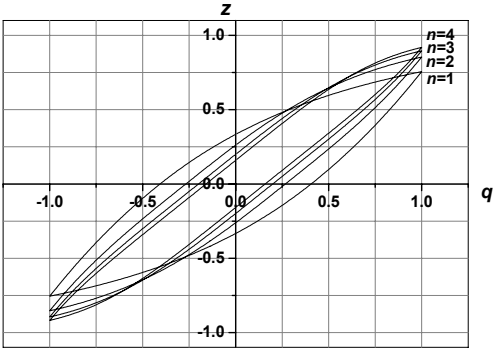

Fig. 2.14. Hysteretic loop dependence on the parameter n (plotted for $\gamma = 0.9$, $\nu = 0.1$, $A = 1$) (copyright Publishing House of the Romanian Academy (2002), reproduced from Giuclea M, Sireteanu T, Mita AM, Ghita G, Genetic algorithm for parameter identification of Bouc–Wen model, Rev Roum Sci Techn Mec Appl, Vol 51, N 2, pp 179–188, used by permission)

As Figure 2.14 (plotted for $\gamma = 0.9$, $\nu = 0.1$, $A = 1$) shows, the variation is significant for small values of n (between 1 and 2 in the numerical example of Figure 2.14), while for larger values ($n > 2$) its effect is negligible.

2.4 Bouc–Wen Parameters Identification

The Bouc–Wen model has the ability to portray a wide range of hysteretic behaviour and by an appropriate choice of the equation coefficients both the slope variation of the stiffness characteristic and the energy dissipated per cycle can be precisely established. The Bouc–Wen equation can be readily combined with plant differential equations to yield an overall dynamic model.

The shape of the Bouc–Wen hysteretic loop depends on the four parameters γ, ν, A and n whose physical meaning has been discussed above. However their identification is not straightforward as the dependence between z and the set of the four parameters is strongly nonlinear and not easy to investigate analytically; furthermore the parameter variation ranges are different. Parameter identification through least-square-based methods is a possible avenue, but may not be the best choice. Black-box optimisation methods based on artificial intelligence techniques such as genetic algorithms (GA) could also be beneficial. Such a method will be employed in Chapter 6 in the context of MRD parameters identification. The method is here briefly introduced. The reader interested in furthering the topic can refer to the textbook of Goldberg (1989).

A GA is a probabilistic search technique inspired from the evolution of species. Such an optimisation tool has an inherent parallelism and ability to avoid stagnation in local optima. It starts with a set of potential solutions called individuals and evolves towards better solutions with respect to an objective function. Genetic operators are defined (namely crossover, mutation and selection) and their application drives the solution towards the optimum. The main elements of a standard GA are genetic representation for potential solutions, an objective function, genetic operators, characteristic constants such as population size, probability of applying an operator, number of children and so forth.

The Bouc–Wen coefficients search problem can be stated as finding a set of parameters γ, ν, A and n such that the Bouc–Wen model given by Equation 2.6 determines a hysteretic curve which is a good approximation of an experimental one, knowing the imposed displacement $q(t)$ and a set of measured data $(q_i, z^*_i)_{i=1,\ldots,n}$ corresponding to a complete cycle.

2.5 Vehicle Ride Models

A broad variety of vehicle mathematical models of increasing degree of complexity has been developed over the years by automotive engineers to provide reliable models for computer-aided automotive design and vehicle performance assessement.

From a purely mathematical standpoint vehicle models can be categorised as distributed models (*i.e.*, governed by partial differential equations) and lumped parameter models (*i.e.*, governed by ordinary differential equations). The former are mainly of interest to vehicle design rather than control algorithm design. Distributed models (typically solved numerically with finite-element-based methods) are widely employed in mechanical, thermal, aerodynamic analyses as well as crashworthiness analyses. For car dynamics (ride and handling) and control studies, lumped parameter models are usually employed. They typically aim to model either ride or handling dynamics or both. In this book only lumped parameter models will be considered.

A car can be thought as being composed of two main subsystems: the sprung mass (chassis) and the unsprung masses (wheels, axles and linkages), connected via a number of elastic and dissipative elements (suspensions, tyres *etc.*) and subjected to external inputs coming from the road profile, the steering system and other external disturbances (*e.g.*, wind gust).

The motion of a vehicle with the nonholonomic constraint of the road has six degrees of freedom (6DOF), classified as follows:

- longitudinal translation (forward and backward motion)
- lateral translation (side slip)
- vertical translation (bounce or heave)
- rotation around the longitudinal axis (roll)
- rotation around the transverse axis (pitch)
- rotation around the vertical axis (yaw)

Vehicle ride is essentially concerned with car vertical dynamics (bounce, pitch, roll) whereas handling is concerned with lateral dynamics (side slip, yaw, roll). Ride models are typically composed of interconnected spring–mass–damper systems and defined by a set of ordinary differential equations.

The most trivial representation of a vehicle suspension has 1DOF. In this simple model the chassis (body) is represented by a mass and the suspension unit by a spring and a damper. Tyre mass and stiffness are neglected as well as any cross-coupling dynamics.

By incorporating a wheel into the model, a more accurate representation having 2DOF (typically referred to as a quarter car model) can be developed. This model was (and still is) very popular in the automotive engineering community, especially before the widespread use of computer simulation, the reason being that the quarter car model, despite its simplicity, features the main variables of interest to suspension performance assessment: body acceleration, dynamic tyre force and suspension working space (Sharp and Hassan, 1986). A merit of the quarter car is that it permits to evaluate more straightforwardly the effects of modifications in control parameters because higher-order dynamics and cross-coupling terms with the other suspension units are not taken into account. A good suspension design should produce improvement of both vehicle road holding and passenger comfort (or possibly improvement of one without degradation of the other), although inherent trade-offs are unavoidable in the design of a passive suspension system.

The quarter car is a 2DOF system having two translational degrees of freedom. Another classical model can be obtained with only 2DOF: the half vehicle model

having a translational degree of freedom and a rotational degree of freedom to describe, respectively, bounce and pitch motions or, analogously, bounce and roll motions (in the former case the model is referred to as a bicycle model). Its natural extension is a 4DOF model, which also includes tyre masses and elasticity. This model can be employed to study the vehicle pitch (or roll) behaviour. However the 4DOF model cannot take into account the cross-couplings between the right- and left-hand side of the car (or front and rear in the case of roll motion). These interactions can be taken into account only by using a 7DOF model (sometimes referred to as a full car model), which allows to represent bounce, roll and pitch motions.

The models mentioned above are classical ride models. Higher order ride models can be developed including further degrees of freedom, *e.g.*, accounting for seat and engine mounting elasticity. Driver and passengers can be modelled as well with springs, masses and damping elements. This is particularly important for accurate human comfort studies. Chapter 3 will deal with this topic in detail.

Analogously to ride vehicle models, also handling models having different degrees of complexity can be developed. The equivalent handling model of the quarter car is a linear single track model which describes lateral and yaw dynamic responses to handling manoeuvres (ignoring the effect of sprung and unsprung masses).

Models including both ride and handling dynamics are necessary when there is a need to accurately investigate the interaction between ride and handling (during a turning manoeuvre, for instance) and to study the limit of handling characteristics or elements such as anti-roll bars. Multibody techniques allow relatively easy development of complicated models with many degrees of freedom. In 1991, Zeid and Chang described a 64DOF model. Models with hundreds of degrees of freedom have been developed by automotive engineers. Such involved models, however, despite their sophistication, suffer from two main drawbacks: parameter uncertainty and long simulation running time. For these reasons they are not always the best choice for control design. Especially in the early stages of the design, a less complicated model is preferable, reserving the use of higher-order models for further refinements and optimisations.

Analogously to cars, several heavy and trailed vehicles (tractor/semi-trailer) models (Gillespie,1992; Wong, 1993) have been developed to examine their ride comfort, tractor–trailer interactions, dynamic tyre forces and road damage. A survey can be found in Jiang *et al.* (2001). These vehicle models usually include linear tyre models, linear or nonlinear suspension characteristics, tandem or single axles. Other truck ride models include suspended tractor cab and driver seat with linear or non-linear components.

The models described and the simulation results presented in this book are based on the use of MATLAB® and Simulink® software. In the following sections the classical vehicle and truck models will be briefly revised.

2.5.1 Quarter Car Model

The quarter car has for a long time been the *par excellence* model used in suspension design. It is a very simple model as it can only represent the bounce

motion of chassis and wheel without taking into account pitch or roll vibration modes. However it is very useful for a preliminary design: it is described by the following system of second-order ordinary differential equations (Figure 2.15; tyre damping is not shown in the figure):

$$m_1\ddot{x}_1 = -2\xi\omega_1(\dot{x}_1 - \dot{x}_2) - k_s(x_1 - x_2), \tag{2.7a}$$

$$m_2\ddot{x}_2 = 2\xi\omega_1(\dot{x}_1 - \dot{x}_2) + k_s(x_1 - x_2) - k_t(x_2 - z_0) - c_t(\dot{x}_2 - \dot{z}_0). \tag{2.7b}$$

If relative displacement is defined as $x = x_1 - x_2$, Equations 2.7a and 2.7b can be rewritten in a more compact form:

$$m_1\ddot{x}_1 = -2\xi\omega_1\dot{x} - k_s x, \tag{2.8a}$$

$$m_2\ddot{x}_2 = 2\xi\omega_1\dot{x} + k_s x - k_t(x_2 - z_0) - c_t(\dot{x}_2 - \dot{z}_0). \tag{2.8b}$$

From the analysis of the quarter car model equations some fundamental properties of the passive suspensions can be analytically evinced and it is possible to quantify the compromise when reduction of both chassis acceleration, suspension working space (sometimes referred as rattle space) and tyre deflection is pursued: the

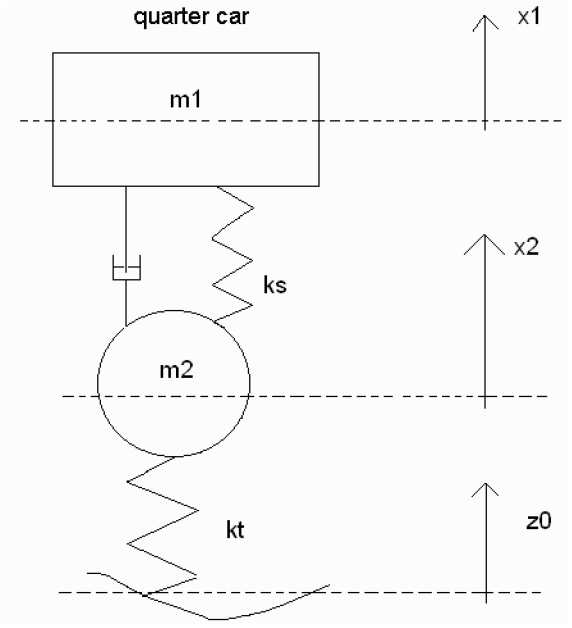

Fig. 2.15. Quarter car model (copyright Inderscience (2005) reproduced with minor modifications from Guglielmino, E, Stammers CW, Stancioiu D and Sireteanu T, Conventional and non-conventional smart damping systems, Int J Vehicle Auton Syst, Vol. 3, N 2/3/4, pp 216–229, used by permission)

quarter car is a dynamic system composed of two interconnected subsystems and as such is subject to constraint equations, independent of the type of interconnections. From the analysis of the quarter car model Hedrick and Butsuen (1988) showed that only three transfer functions can be independently defined and that invariant points (*i.e.*, values at specified frequencies depending only on k_t, m_1 and m_2 but not on k_s) exist at particular frequencies. In particular they showed that the acceleration transfer function has an invariant point at the wheel-hop frequency. Similarly, the suspension deflection transfer function has an invariant point at the rattle space frequency. The trade-off between passenger comfort and suspension deflection occurs because it is not possible to simultaneously keep both transfer functions small around the wheel-hop frequency in the low-frequency range.

2.5.2 Half Car Model

Pitch motion can be taken into account with the half vehicle model (also known as the bicycle model). The governing equations are the following (Figure 2.16), with α representing pitch:

$$\begin{cases} m\ddot{x} = -k_2(z - b\alpha - z_4) - k_1(z + a\alpha - z_3) - c_2(\dot{z} - b\dot{\alpha} - \dot{z}_4) - c_1(\dot{z} + a\dot{\alpha} - \dot{z}_3), \\ J\ddot{\alpha} = k_2(z - b\alpha - x_4)b - k_1(x + a\alpha - z_3)a - c_2(\dot{z} - b\dot{\alpha} - \dot{z}_4)b - c_1(\dot{z} + a\dot{\alpha} - \dot{z}_3)a, \\ m_1\ddot{z}_3 = k_1(z + a\alpha - z_3) - k_{01}(z_3 - z_{01}) + c_1(\dot{z} + a\dot{\alpha} - \dot{z}_3), \\ m_2\ddot{z}_4 = k_2(z - b\alpha - z_4) - k_{02}(z_4 - z_{02}) + c_2(\dot{z} - b\dot{\alpha} - \dot{z}_4), \end{cases} \tag{2.9}$$

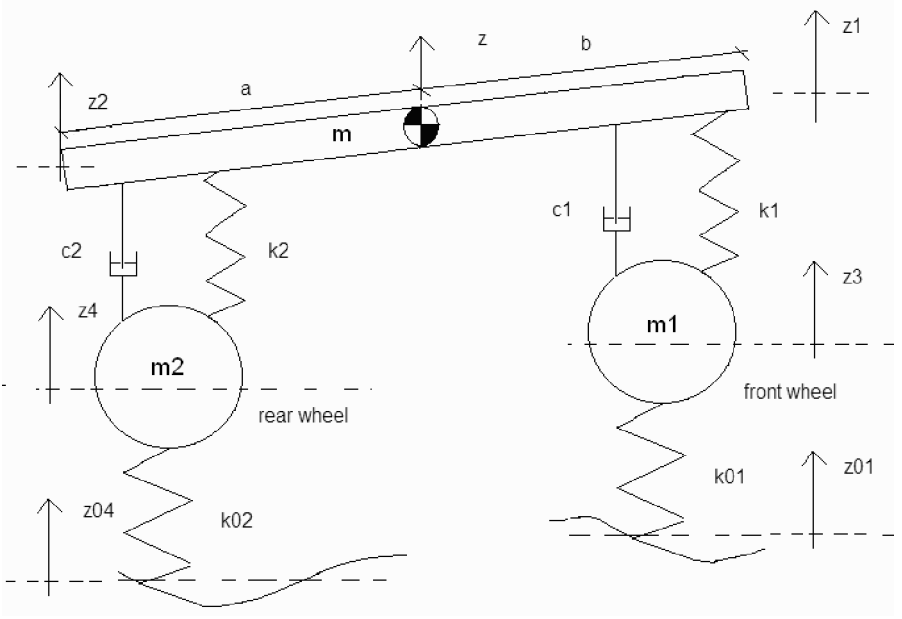

Fig. 2.16. Half car model with 4DOF

where m is the sprung mass, m_1, m_2 the front and rear unsprung masses, J the pitch inertia, and a and b the distances of the front and rear of the vehicle from its centre of gravity. Replacing α with the roll angle, pitch inertia J by roll inertia and b by half-track length this model can be also employed to describe roll motion.

2.5.3 Full Car Model

The 7DOF vehicle ride model (Sireteanu *et al.*, 1981) extends the half car model to the entire vehicle: 3DOF are used for the sprung mass (bounce, roll and pitch), while the unsprung masses have 4DOF (1DOF for each tyre), as depicted in Figure 2.17. The governing equations can be written compactly in matrix form (bold letters denote matrices and vectors):

$$\boldsymbol{M}\ddot{\boldsymbol{q}} + \boldsymbol{P}^T\boldsymbol{C}\boldsymbol{P}\dot{\boldsymbol{q}} + \boldsymbol{P}^T\boldsymbol{K}\boldsymbol{P}\boldsymbol{q} + \boldsymbol{F}_d = -\boldsymbol{P}^T\boldsymbol{K}_0\boldsymbol{z}_0 - \boldsymbol{P}^T\boldsymbol{C}_0\dot{\boldsymbol{z}}_0\,, \tag{2.10}$$

with $\boldsymbol{q}\in\Re^7$, $\boldsymbol{z_0}\in\Re^4$, $\boldsymbol{F_d}\in\Re^7$, $\boldsymbol{M}\in\Re^{7x7}$, $\boldsymbol{K}\in\Re^{8x8}$, $\boldsymbol{C}\in\Re^{8x8}$, $\boldsymbol{K_0}\in\Re^{8x4}$, $\boldsymbol{C_0}\in\Re^{8x4}$ and $\boldsymbol{P}\in\Re^{8x7}$.

The vertical displacement vector $\boldsymbol{z}\in\Re^8$ is defined as:

$$\boldsymbol{z} = [z_1\,, z_2\,, z_3\,, z_4\,, z_5\,, z_6\,, z_7, z_8]^T \tag{2.11}$$

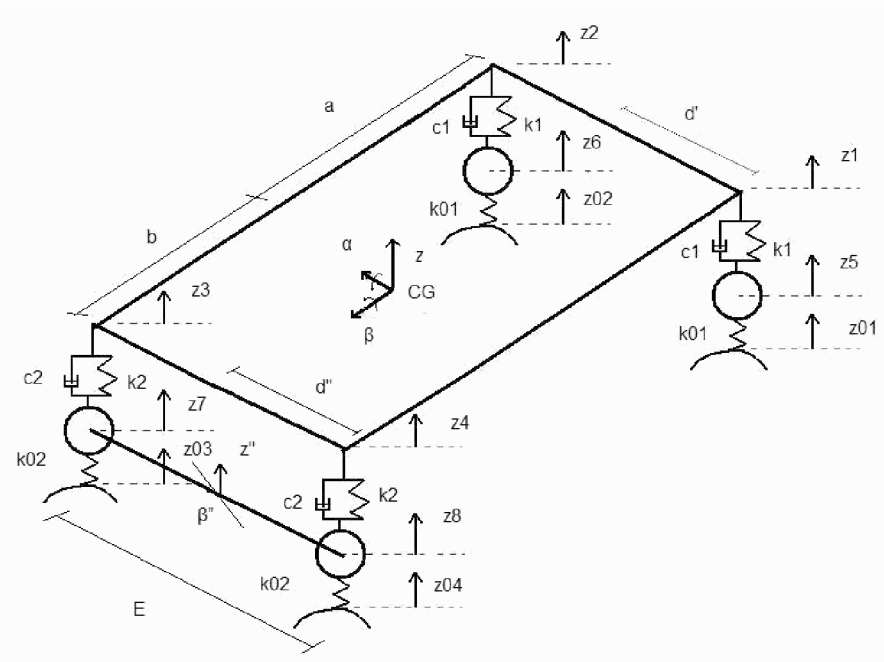

Fig. 2.17. Full car model with 7DOF (copyright ASME (2001), reproduced with minor modifications from from Guglielmino E, Edge KA, Modelling of an electrohydraulically-activated friction damper in a vehicle application, Proc ASME IMECE 2001, New York, used by permission)

(the vertical displacements are not all independent).

Let $\boldsymbol{q}$ be the vector of generalised co-ordinates:

$$\boldsymbol{q} = [q_1, q_2, q_3, q_4, q_5, q_6, q_7]^T \tag{2.12}$$

with the following choice of co-ordinates:

$$q_1 = z\,;\; q_2 = z_5\,;\; q_3 = z_6\,;\; q_4 = z''\,;\; q_5 = \alpha\,;\; q_6 = \beta\,;\; q_7 = \beta'', \tag{2.13}$$

z and $\boldsymbol{q}$ being related by the matrix $\boldsymbol{P}$, dependent upon the vehicle geometry:

$$z = \boldsymbol{P}\boldsymbol{q}. \tag{2.14}$$

Consider the vertical displacement vector and the matrix $\boldsymbol{P}$ being defined as:

$$\boldsymbol{P} = \begin{bmatrix} 1 & 0 & 0 & 0 & -a & d' & 0 \\ 1 & 0 & 0 & 0 & -a & -d' & 0 \\ 1 & 0 & 0 & 0 & b & d'' & 0 \\ 1 & 0 & 0 & 0 & b & -d'' & 0 \\ 0 & 1 & 0 & 0 & 0 & 0 & 0 \\ 0 & 0 & 1 & 0 & 0 & 0 & 0 \\ 0 & 0 & 0 & 1 & 0 & 0 & \frac{E}{2} \\ 0 & 0 & 0 & 1 & 0 & 0 & -\frac{E}{2} \end{bmatrix}, \tag{2.15}$$

where a and b are the distances of the front and rear of the vehicle from its centre of gravity, d' and d'' are, respectively, the front and rear half-track lengths and E the inter-wheel distance.

The road input vector z_0 is then defined as:

$$\boldsymbol{z_0} = [z_{01}, z_{02}, z_{03}, z_{04}]^T. \tag{2.16}$$

Equation 2.10 can be obtained using Lagrangian formalism. The Lagrange equations, expressed as a function of the kinetic energy are:

$$\frac{\mathrm{d}}{\mathrm{d}t}\frac{\partial T}{\partial \dot{q}_k} - \frac{\partial T}{\partial q_k} = g_k \qquad k=1,\ldots,7 \tag{2.17}$$

where T is the total kinetic energy of the system, defined by the quadratic form

$$T = \frac{1}{2}\dot{\boldsymbol{q}}^T \boldsymbol{M}\dot{\boldsymbol{q}}, \tag{2.18}$$

$\boldsymbol{M}$ being the mass matrix:

$$\boldsymbol{M} = \text{diag}(m,\ m_1,\ m_1,\ m_2,\ J_\alpha,\ J_\beta,\ J_{\beta''}), \tag{2.19}$$

where m is the sprung mass, m_1 , m_2 the front and rear unsprung masses, J_α the pitch inertia and J_β and $J_{\beta''}$ the roll inertias of sprung mass and rear inter-axis bar.

The right-hand side of Equation 2.17 is defined as:

$$g_k = \sum_{i=1}^{8} f_i \frac{\partial x_i}{\partial q_k} \quad k=1,\ldots, 7. \tag{2.20}$$

Defining the vector $\boldsymbol{f}$ of the forces applied to sprung and unsprung masses

$$\boldsymbol{f} = [\boldsymbol{f}_1\ ,\ \boldsymbol{f}_2\ ,\ \boldsymbol{f}_3\ ,\ \boldsymbol{f}_4\ ,\ \boldsymbol{f}_5\ ,\ \boldsymbol{f}_6\ ,\ \boldsymbol{f}_7,\ \boldsymbol{f}_8\ ]^T. \tag{2.21}$$

the forces applied to sprung and unsprung masses are:

$$\boldsymbol{f} = -[\boldsymbol{K}\boldsymbol{z} + \boldsymbol{C}\dot{\boldsymbol{z}} + \boldsymbol{K}_{\boldsymbol{0}}\boldsymbol{z}_{\boldsymbol{0}} + \boldsymbol{C}_{\boldsymbol{0}}\dot{\boldsymbol{z}}_{\boldsymbol{0}}\ ], \tag{2.22}$$

where $\boldsymbol{K}$ is the stiffness matrix:

$$\boldsymbol{K} = \begin{bmatrix} k_1 & 0 & 0 & 0 & -k_1 & 0 & 0 & 0 \\ 0 & k_1 & 0 & 0 & 0 & -k_1 & 0 & 0 \\ 0 & 0 & k_2 & 0 & 0 & 0 & -k_2 & 0 \\ 0 & 0 & 0 & k_2 & 0 & 0 & 0 & -k_2 \\ -k_1 & 0 & 0 & 0 & k_1 + k_{01} & 0 & 0 & 0 \\ 0 & -k_1 & 0 & 0 & 0 & k_1 + k_{01} & 0 & 0 \\ 0 & 0 & -k_2 & 0 & 0 & 0 & k_2 + k_{02} & 0 \\ 0 & 0 & 0 & -k_2 & 0 & 0 & 0 & k_2 + k_{02} \end{bmatrix} \tag{2.23}$$

and $\boldsymbol{K}_{\boldsymbol{0}}$ is the unsprung mass stiffness matrix

$$\boldsymbol{K_0} = \begin{bmatrix} 0 & 0 & 0 & 0 \\ 0 & 0 & 0 & 0 \\ 0 & 0 & 0 & 0 \\ 0 & 0 & 0 & 0 \\ -k_{01} & 0 & 0 & 0 \\ 0 & -k_{01} & 0 & 0 \\ 0 & 0 & -k_{02} & 0 \\ 0 & 0 & 0 & -k_{02} \end{bmatrix}. \tag{2.24}$$

Analogous definitions can be given for matrices $\boldsymbol{C}$ and $\boldsymbol{C_0}$, the latter being the tyre damping matrix, usually negligible (tyre damping is not depicted in Figure 2.17).

Combining Equations 2.14 and 2.18 yields:

$$x_k = \sum_{i=1}^{7} p_{ik} q_k \quad k=1,\ldots, 8, \tag{2.25}$$

$$T = \frac{1}{2} \sum_{i=1}^{7} m_{kk} \dot{q}_k^2. \tag{2.26}$$

Developing (2.17) yields:

$$g_k = \sum_{i=1}^{8} p_{ik} q_k = (P^T f) \quad k=1,\ldots, 7, \tag{2.27}$$

$$\frac{\mathrm{d}}{\mathrm{d}t} \frac{\partial T}{\partial \dot{q}_k} = (M\ddot{q})_k \qquad k=1,\ldots, 7, \tag{2.28}$$

hence

$$\boldsymbol{M\ddot{q}} = \boldsymbol{P}^{\tau} \boldsymbol{f} \ . \tag{2.29}$$

Taking into account Equation 2.22, the governing Equation 2.10 is obtained:

$$\boldsymbol{M\ddot{q}} + \boldsymbol{P^T C P \dot{q}} + \boldsymbol{P^T K P q} + \boldsymbol{F_d} = -\boldsymbol{P^T K_0 z_0} - \boldsymbol{P^T C_0 \dot{z}_0} \, . \tag{2.30}$$

In the model here described, front suspensions are taken to be independent and rear suspensions dependent (connected through a rigid axle). However the model

can be easily modified to represent independent front suspensions or both front and rear dependent suspensions, by appropriate choices of the matrices ***M***, ***K*** and ***C***.

2.5.4 Half Truck Model

The half truck model is the equivalent of the half vehicle model for an articulated vehicle, and has seven degrees of freedom. Figure 2.18 depicts a schematic of the truck model (Tsampardoukas *et al.*, 2007)

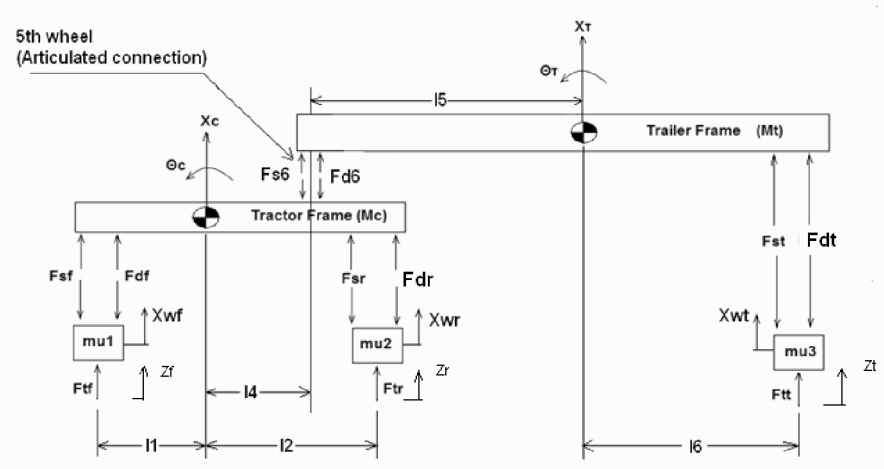

Fig. 2.18. Half truck model (copyright Elsevier, reproduced from Tsampardoukas G, Stammers CW and Guglielmino E, Hybrid balance control of a magnetorheological truck suspension, accepted for publication in Journal of Sound and Vibration, used by permission)

It is composed of two sprung masses, namely the tractor body (or frame) and the trailer body, together with three unsprung masses (the three wheels). The tractor and the trailer are linked through an articulated connection known as the fifth wheel. Two vibration modes are considered for each sprung unit (heave and pitch) and one for the unsprung masses (heave).

The governing equations can be readily obtained by consideration of forces and moments as follows:

$$\begin{cases} m_{\mathrm{c}}\ddot{x}_{\mathrm{c}} = F_{\mathrm{sf}} + F_{\mathrm{df}} + F_{\mathrm{sr}} + Fc_{\mathrm{rear}} - F_{\mathrm{s6}} - F_{\mathrm{d6}} \\ J_{\mathrm{c}}\ddot{\theta}_{\mathrm{c}} = F_{\mathrm{sr}} l_2 + Fc_{\mathrm{rear}} l_2 - F_{\mathrm{s6}} l_4 - F_{\mathrm{d6}} l_4 - F_{\mathrm{sf}} l_1 - F_{\mathrm{df}} l_1 \\ m_{\mathrm{t}}\ddot{x}_{\mathrm{t}} = F_{\mathrm{st}} + Fc_{\mathrm{trailer}} + F_{\mathrm{s6}} + F_{\mathrm{d6}} \\ J_{\mathrm{t}}\ddot{\theta}_{\mathrm{t}} = F_{\mathrm{st}} l_6 + Fc_{\mathrm{trailer}} l_6 - F_{\mathrm{s6}} l_5 - F_{\mathrm{d6}} l_5 \\ m_{\mathrm{u1}}\ddot{x}_{\mathrm{wf}} = F_{\mathrm{tf}} - F_{\mathrm{sf}} - F_{\mathrm{df}} \\ m_{\mathrm{u2}}\ddot{x}_{\mathrm{wr}} = F_{\mathrm{tr}} - F_{\mathrm{sr}} - F_{\mathrm{dr}} \\ m_{\mathrm{u3}}\ddot{x}_{\mathrm{wt}} = F_{\mathrm{tt}} - F_{\mathrm{st}} - F_{\mathrm{dt}} \end{cases} \tag{2.31}$$

where

$$F_{\mathrm{sf}} = k_f(x_{\mathrm{wf}} - x_{\mathrm{c}} + l_1\theta_{\mathrm{c}})$$
$$F_{\mathrm{df}} = c_f(\dot{x}_{\mathrm{wf}} - \dot{x}_{\mathrm{c}} + l_1\dot{\theta}_{\mathrm{c}})$$

$$F_{\mathrm{sr}} = k_r(x_{\mathrm{wr}} - x_{\mathrm{c}} - l_2\theta_{\mathrm{c}})$$
$$F_{\mathrm{dr}} = c_r(\dot{x}_{\mathrm{wr}} - \dot{x}_{\mathrm{c}} - l_2\dot{\theta}_{\mathrm{c}})$$

$$F_{\mathrm{st}} = k_t(x_{\mathrm{wt}} - x_{\mathrm{t}} - l_6\theta_{\mathrm{t}})$$
$$F_{\mathrm{dt}} = c_t(\dot{x}_{\mathrm{wt}} - \dot{x}_{\mathrm{t}} - l_6\dot{\theta}_{\mathrm{t}})$$

$$F_{\mathrm{s6}} = k_5(x_{\mathrm{c}} + l_2\theta_{\mathrm{c}} - x_{\mathrm{t}} + l_5\theta_{\mathrm{t}})$$
$$F_{\mathrm{d6}} = c_5(\dot{x}_{\mathrm{c}} + l_2\dot{\theta}_{\mathrm{c}} - \dot{x}_{\mathrm{t}} + l_5\dot{\theta}_{\mathrm{t}})$$

$$F_{\mathrm{tf}} = k_{\mathrm{tf}}(z_{\mathrm{f}} - x_{\mathrm{wf}})$$
$$F_{\mathrm{tr}} = k_{\mathrm{tr}}(z_{\mathrm{r}} - x_{\mathrm{wr}})$$
$$F_{\mathrm{tt}} = k_{\mathrm{tt}}(z_{\mathrm{t}} - x_{\mathrm{wt}})$$

$$rear\_relative\_velocity = (\dot{x}_{\mathrm{c}} + l_2\dot{\theta}_{\mathrm{c}} - \dot{x}_{\mathrm{wr}})$$

$$trailer\_relative\_velocity = (\dot{x}_{\mathrm{t}} + l_6\dot{\theta}_{\mathrm{t}} - \dot{x}_{\mathrm{wt}})$$

$$z_{\mathrm{f}} = front\_wheel\_input$$
$$z_{\mathrm{r}} = rear\_wheel\_input$$
$$z_{\mathrm{t}} = trailer\_wheel\_input$$

(2.32)

The equations can be implemented in Simulink®. Figure 2.19 shows a schematic of the Simulink® model. The meaning of the symbols in Equations 2.31 and 2.32 are listed in Table 2.1.

Table 2.1. Truck model symbols notation (copyright Elsevier, reproduced from Tsampardoukas G, Stammers CW and Guglielmino E, Hybrid balance control of a magnetorheological truck suspension, accepted for publication in Journal of Sound and Vibration, used by permission)

F_{sf}	Front tractor suspension spring force
F_{df}	Front tractor suspension damping force
F_{sr}	Rear tractor suspension spring force
F_{dr}	Rear tractor suspension damping force
F_{st}	Trailer suspension spring force
F_{dt}	Trailer suspension damping force
F_{s6}	Fifth wheel spring force
F_{d6}	Fifth wheel damping force
x_t	Trailer heave
x_c	Tractor heave
ϑ_c	Tractor pitch
ϑ_t	Trailer pitch
x_{wf}	Front tractor wheel heave
x_{wr}	Rear tractor wheel heave
x_{wt}	Trailer tractor wheel heave
z_f	Front tractor road input
z_r	Rear tractor road input
z_t	Trailer road input
F_{tf}	Excitation force (front tractor)
F_{tr}	Excitation force (rear tractor)
F_{tt}	Excitation force (trailer)

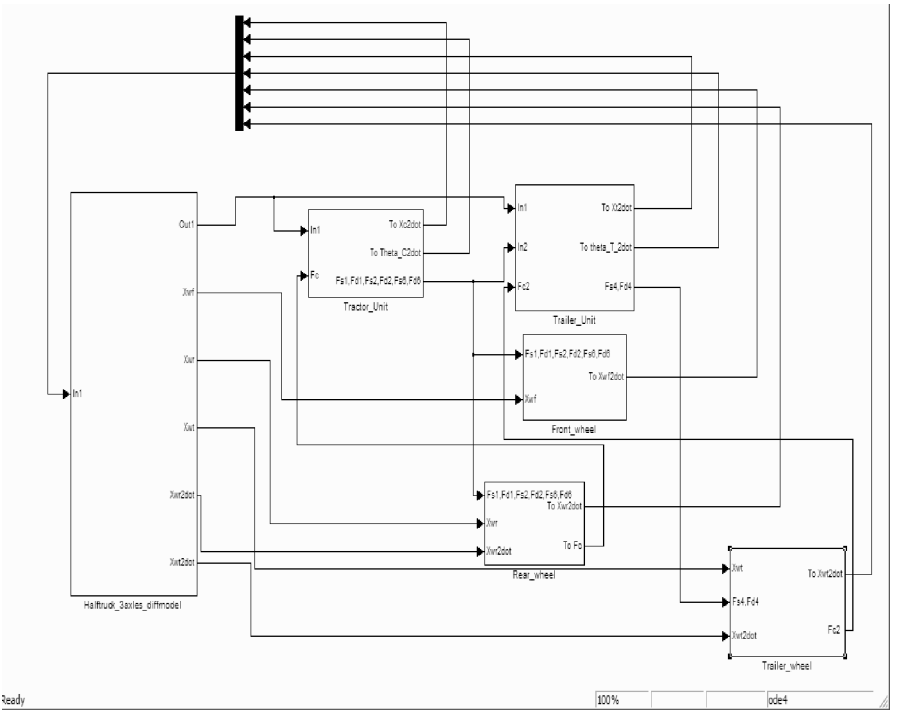

Fig. 2.19. Simulink® half truck model

2.6 Tyre Modelling

Tyres are made of rubber, *i.e.*, a viscoelastic material and in ride studies the vertical tyre stiffness can be approximated by a spring and some damping (either pure viscous or hysteretic damping, but often negligible). In the vehicle models described so far, the tyre has been represented as a spring (and a viscous damper term). This model although quite crude is acceptable for ride analysis. In handling, braking or traction studies more sophisticated models are required which account for road–tyre adhesion (both longitudinal and lateral) as well as rolling friction. A classical model is the so-called Pacejka magic formula (Pacejka and Bakker, 1991). At higher frequencies and for short road obstacles even more sophisticated models are required.

The majority of workers utilise a point contact model since it is easy to use. Such a model has at least two defects. Firstly, the point follows the slightest vertical excursion of the road and hence generates high-frequency inputs which in practice would not occur as the tyre contact patch bridges or envelops such points.

Secondly, such a model cannot generate longitudinal forces although it is evident that these exist to a greater or lesser degree. Indeed such a model cannot predict the deceleration of a vehicle on a steady incline.

A more useful model is a radial spring tyre model (Smith, 1977; Bernard *et al.*, 1981; Crolla *et al.*, 1984). The number of springs needed is not obvious, and depends on the type of road surface; the authors (unpublished work) have found 360 to be adequate. The stiffness of the springs is adjusted to produce a prescribed static deflection.

For on-road applications, it is valid to regard the road profile as rigid compared to the flexible tyre. The chief difficulty is locating the point of contact for each spring when a pseudo-random road profile is assumed. Such a model generates longitudinal forces but does not admit enveloping, although Davis (1974) has extended the model to allow for this. Torsional tyre distortion is not modelled.

2.7 Road Modelling

The representation of the road profile is vital for vehicle dynamic simulations because it is the main source of excitation. An accurate road model is as important as a good vehicle model. Sources of vehicle vibration include forces induced by road surface irregularities as well as aerodynamic forces and vibration that arise from the rotating mechanical parts of the vehicles (tyres, engine and transmission). However, the road surface elevation profile (identified by the co-ordinates z_{0i}, in the previous models) plays the major role. Road roughness includes any type of surface irregularities from bump and potholes to small deviations.

The reduction of forces transmitted to the road by moving vehicles (particularly for heavy vehicles) is also an important issue responsible for road damage. Heavy-vehicle suspensions should be designed accounting also for this constraint. The issue will be dealt in detail in a case study in Chapter 7.

Road inputs can be classified into three types: deterministic road (periodic and almost-periodic) inputs, random-type inputs and discrete events such as bumps and potholes.

As far as deterministic inputs are concerned, a variety of periodical waveforms can be used, such as sine waves, square waves or triangular waves. To a first approximation the road profile can be assumed to be sinusoidal. Although not realistic, it is useful in a preliminary study because it readily permits a comparison of the performance of different suspension designs both in the time and in the frequency domain (through transmissibility charts, plotted at different frequencies).

A multi-harmonic input which is closer to an actual road profile can be generated. A possible choice which approximates fairly well a real road profile is a so-called pseudo-random input (Sayers and Karamihas, 1998; Dukkipati, 2000) which results from summing several non-commensurately related sine waves (*i.e.*, the ratio of all possible pairs of frequencies is not a rational number) of decreasing amplitude, so as to provide a discrete approximation of a continuous spectrum of a random input. The trend can be proved to be non-periodic (sometimes referred to as almost periodic) in spite of being a sum of periodic waveforms (Bendat and

Piersol, 1971). To achieve a pseudo-random profile effect it is advisable to select spatial frequencies of the form

$$j\Delta\Omega + \text{trascendental term} \quad j=1,\ldots, m. \tag{2.33}$$

where j is an integer, $\Delta\Omega$ is the separation between spatial frequencies and the added term could be $e/1000$ or $\pi/1000$ for example. The spatial frequency range is $(m\text{-}1)\ \Delta\Omega$. The RMS amplitude at each centre frequency is obtained from the power spectral law and multiplication by $\Delta\Omega$.

Another possible way to generate a realistic multi-harmonic input consists in making the ratio between frequencies constant and decreasing with amplitude, but using randomly generated phase angles (between 0 and 360 degrees) for each component. In this case the resulting waveform is periodical. Simulation results presented subsequently are based on the latter approach.

Figure 2.20 shows an example of road profile: 20 sine waves with random phases have been added together in order to create a pseudo-random profile. The amplitude of the profile is calculated to approximate a smooth highway by using the spatial frequency data suggested by the Society of Automotive Engineers (SAE).

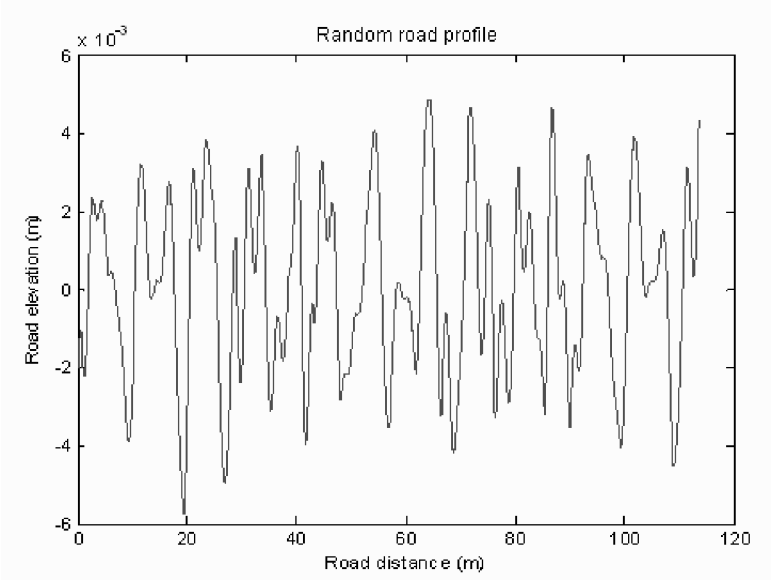

Fig. 2.20. Pseudo-random road profile

However, these road profiles are deterministic functions and as a consequence could not represent a real random pavement.

A stochastic model gives the more realistic representation of a road profile. The power spectral density (PSD) is the most common way to characterise the road

roughness (British standard BS 7853, 1996). A road could well be approximated (Wong, 1993) by an ergodic process with spectral density expressed by:

$$S(\Omega) = C\Omega^{-n}, \tag{2.34}$$

where Ω is the spatial frequency, having units of cycles/m (*i.e.*, Ω is the inverse of wavelength), C is a coefficient dependent on the road roughness, f the frequency in Hz and n is a rational exponent. It follows that $\Omega=f/V$, where V is the forward speed of the car, so that:

$$S(f) = (\frac{C}{V^{-n}})f^{-n}. \tag{2.35}$$

This approach involves an analysis in terms of power spectral densities. For a linear system the input and output spectral densities $Y_{in}(f)$ and $Y_{out}(f)$ are related through the transfer function of the system $G(f)$, from the equation:

$$Y_{out}(f) = \left|G(f)\right|^2 Y_{in}(f). \tag{2.36}$$

This property in the frequency domain only applies to linear systems and allows the output spectral density to be readily calculated if the vehicle transfer function and the input spectral density are known. For a nonlinear system this property does not hold.

Several techniques (Cebon, 1996) exist to characterise the road roughness by using spectral densities. For example, the inverse discrete Fourier transform (DFT) can be used to generate a single road profile. Alternatively a two-dimensional inverse DFT can be employed to create a pair of correlated road profiles for full vehicle simulation. Tyre envelopment can be added to the models.

Discrete events such as bumps or potholes cannot be modelled with the approaches described above and are instead usually modelled using half-sine waves or also using the Heavyside function.